Heat-Induced Phase Transition and Crystallization of Hydrophobically End-Capped Poly(2-isopropyl-2-oxazoline)s in Water

ARTICLE *in* MACROMOLECULES · AUGUST 2009

Impact Factor: 5.8 · DOI: 10.1021/ma900838v

3 AUTHORS, INCLUDING:

Francoise Winnik
Université de Montréal
272 PUBLICATIONS **13,779** CITATIONS

5818 *Macromolecules* **2009**, *42*, 5818–5828
DOI: 10.1021/ma900838v

Macromolecules
ARTICLE

Heat-Induced Phase Transition and Crystallization of Hydrophobically End-Capped Poly(2-isopropyl-2-oxazoline)s in Water

Rodolphe Obeid,[†] Fumihiko Tanaka,[‡] and Françoise M. Winnik*,[†]

[†]*Department of Chemistry and Faculty of Pharmacy, University of Montreal, CP 6128 Succursale Centre Ville, Montreal, QC H3C 3J7, Canada, and* [‡]*Department of Polymer Science, Kyoto University, Katsura, Nishikyo-ku, Kyoto 615-8510, Japan*

Received April 16, 2009; Revised Manuscript Received June 8, 2009

ABSTRACT: The phase diagrams of semitelechelic and telechelic hydrophobically modified poly(2-isopropyl-2-oxazolines) (HM-PiPrOx) in water were characterized in terms of an extensive set of parameters: the cloud point (T_{cp}), obtained from turbidity measurements, the transition temperature (T_M) and enthalpy (ΔH), derived from high-sensitivity differential scanning calorimetry (HS-DSC), the coefficient of thermal volume expansion, α, measured by pressure perturbation calorimetry (PPC), together with assessment by X-ray diffraction of the extent of polymer crystallization from hot water. Data were recorded as a function of the molecular weight of the polymers (7000, 10 000, and 13 000 g mol^{-1}), the end-group functionality (α-*n*-octadecyl-ω-hydroxyl- or α,ω-di-*n*-octadecyl-), the polymer concentration (0.1−10 g L^{-1}), and the solvent (H_2O or D_2O). For all polymer solutions, the cloud point temperature was lower than the transition temperature, in agreement with previous studies of telechelic HM-poly(ethylene oxides) and HM-poly(*N*-isopropylacrylamides) aqueous solutions. In solutions of all telechelic HM-PiPrOx and of the semitelechelic HM-PiPrOx 7000 and 10 000 g mol^{-1}, the onset of turbidity was accompanied by an endotherm attributed to a rigid-to-fluid phase transition of the hydrophobic core of the polymeric micelles formed in aqueous solutions kept below T_{cp}. Semitelechelic HM-PiPrOx samples crystallized from water upon prolonged heating at 70 °C, whereas telechelic HM-PiPrOx samples remained amorphous under these conditions. The results are discussed in terms of the dipole−dipole interactions between adjacent PiPrOx chains in the micelle corona which restrict the motion of *n*-octadecyl chains in the micellar core and favor intermicellar interactions. Water molecules acting as hydrogen-bound cross-linker between polymer chains also contribute to intra- and intermicellar PiPrOx chain association.

Introduction

It is generally accepted that, although water exhibits many properties typical of small molecule liquids, it has some unique features attributable to short-range attractive interactions between water molecules through hydrogen bonds. These interactions impose geometrical constraints on the positions of the water molecules and prevent close packing of the molecules.[1] Introducing an amphiphile in water disrupts this organized arrangement, as the water molecules attempt to accommodate their guest. The hydrophilic parts of the amphiphile usually contain polar groups with electronegative atoms that form hydrogen bonds with water, while the hydrophobic sections are driven to self-assemble by a mechanism known as hydrophobic hydration. Association of the hydrophobic groups is opposed by the steric repulsion between the hydrated hydrophilic parts of the solute. The competition between the two forces triggers the formation of specific self-assembled structures, which vary in shape and size depending on the chemical structure of the amphiphile. Hydrophilic polymers end-capped with hydrophobic groups, or telechelic hydrophobically modified (HM) polymers, are among the simplest models to study the self-assembly of polymeric amphiphiles in water.[2,3] They have been studied in great detail, both from the theoretical point of view and experimentally with poly(ethylene oxide) (PEO) terminated with long alkyl groups as a model.[4−6] Their self-assembly in water was shown to depend markedly on polymer concentration and solution temperature. In the dilute regime and at ambient temperature, telechelic HM-polymers form intramolecular loops via end-group association. The loops aggregate into micelles of flowerlike shape or "flower micelles".[7,8] At higher polymer concentration, a few chains start to form bridges between micelles, yielding clusters of micelles. In solutions of even higher concentration, extensive networks form, in which the flower micelles act as junction points connected via bridging chains.[9] The effect of temperature on aqueous telechelic HM-PEO solutions was assessed by François et al.,[10] who observed that the cloud point (T_{cp}, temperature of onset in solution turbidity) of aqueous telechelic HM-PEO solutions is lower by as much as 100 °C compared to the T_{cp} of solutions of the unmodified PEO. This association pattern accounts for the macroscopic properties of aqueous telechelic HM-polymers solutions which, at room temperature, change from low-viscosity liquids to gels upon increasing polymer concentration.[11] Telechelic HM polymers have found numerous applications as rheology modifiers in waterborne fluids, paints, coatings, cosmetics, and foodstuffs.[12] Most industrial telechelic HM-polymers consist of a poly(ethylene oxide) (PEO) chain linked to either alkyl[8,13,14] or perfluoroalkyl end groups.[15,16] Detailed studies on telechelic HM-PEOs have demonstrated that their behavior in solution is sensitive to subtle changes in the chemical structure of the hydrophobic group and also of the linker connecting the end segment to the PEO chain.[17] Less emphasis was placed on the effect of the main-chain structure on the solution properties of telechelic HM polymers, mostly in view of synthetic difficulties associated with the synthesis of well-defined telechelic hydrophilic polymers other than PEO.

*Corresponding author: Ph (514) 340 5179, Fax (514) 340 5292, e-mail francoise.winnik@umontreal.ca.

 Published on Web 07/02/2009

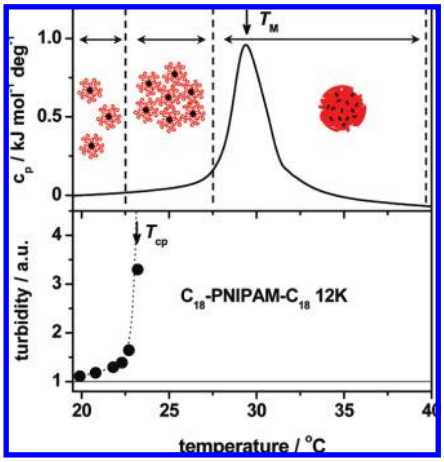

Figure 1. (top) Microcalorimetric endotherms and (bottom) changes with temperature of the light transmittance recorded for an aqueous solution of telechelic HM-PNIPAM (polymer concentration: 5.0 g L^{-1}).

Over the past decade, however, new types of telechelic HM-polymers were reported, including telechelic poly(2-alkyl-2-oxazolines) terminated with alkyl or perfluoroalkyl chains, prepared by living cationic polymerization of 2-alkyl-2-oxazolines[18−21] and HM-poly(*N*-isopropylacrylamide) (PNIPAM) obtained by controlled free radical polymerization of *N*-isopropylacrylamide (NIPAM).[22] Like PEO, PNIPAM is highly soluble in cold water and becomes insoluble when the solution temperature exceeds a specific value, the lower critical solution temperature (LCST, ~32 °C).[23] The T_{cp} of aqueous telechelic HM-PNIPAM solutions is lower than that of PNIPAM. The T_{cp} depression is on the order of 5−10 °C, depending on the length of the PNIPAM chain and on polymer concentration.[22] Interestingly, Kujawa et al.[22] noted that the temperature corresponding to the maximum temperature (T_M) of the endotherm recorded for aqueous telechelic HM-PNIPAM solutions by high sensitivity differential scanning calorimetry (HS-DSC) is systematically different from the T_{cp}, obtained by turbidimetry measurement for the same solution.[22] The phenomenon is exemplified in Figure 1, which presents in the top panel a microcalorimetry scan recorded for a solution of telechelic HM-PNIPAM (M_n = 12 000 g mol^{-1}) and in the bottom panel the heat-induced changes in turbidity of the same solution. The endotherm recorded by microcalorimetry corresponds to the heat released upon dehydration of the polymer chain and reflects the change in solvent quality. The cloud point signals the onset of association of several polymer micelles via formation of intermicellar bridges as a consequence of temperature-dependent concentration fluctuations and progressive changes in solvent quality.[22] Intermicellar association in dilute solution, below the LCST, reflects a gradual enhancement of the interactions between the hydrophilic coronae of the micelles, which change from repulsive to attractive as the solvent quality of water passes from good to poor. This association into larger objects is readily detected by turbidimetry but is not observed by HS-DSC, an indication that the process is athermal, at least within the sensitivity of HS-microcalorimetry (see Figure 1).

The fact that the temperature (T_{cp}), for which micellar association of telechelic HM-polymers begins, differs from the temperature (T_M) of main-chain dehydration and collapse merits further study from the fundamental viewpoint as well as in view of possible practical applications in the design of "smart" temperature-responsive fluids. To test the generality of the phenomenon, we set about to study the temperature-dependent properties of telechelic HM-poly(2-isopropyl-2-oxazolines) (PiPrOx) in water, focusing on the thermodynamics of water/polymer interactions.

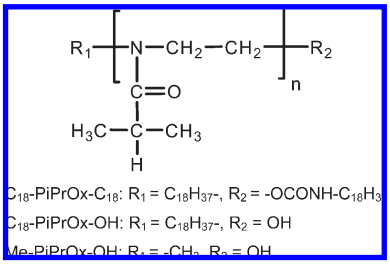

Figure 2. Structure of the polymers in this study.

The homopolymer PiPrOx is a crystalline,[24] nonionic tertiary amide polymer with a $-CH_2N-[CO-CH(CH_3)_2]CH_2-$ repeat unit (Figure 2), which is a structural isomer of PNIPAM. PiPrOx is prepared by cationic ring-opening polymerization of 2-isopropyl-2-oxazoline.[25] It exhibits a wide range of solubility in polar organic solvents, such as tetrahydrofuran, in which it takes a random coil conformation. It is soluble in cold water and separates from solution upon heating past a temperature in the 36−70 °C range, depending on polymer molecular weight and concentration.[26,27] These properties, together with features typical of poly(2-alkyl-2-oxazolines) such as nontoxicity[28] and ease of end-functionalization[18,19,29,30] and of copolymerization,[31−33] justify the renewed interest in this polymer synthesized for the first time 40 years ago. Moreover, it was reported recently that the phase separation of PiPrOx in water is reversible only if the solution is cooled rapidly to room temperature. Prolonged incubation of phase-separated aqueous PiPrOx solutions at ~65 °C triggers crystallization of the PiPrOx chains into fibrils that are insoluble in cold water.[34,35] The exact mechanism of the crystallization of hot PiPrOx coagulates is still poorly understood. It has been attributed to favorable dipolar interactions between the amide dipoles, coupled with nonspecific hydrophobic interactions between the nonpolar isopropyl groups.[35] That PiPrOx crystallizes from its coagulate while its structural isomer PNIPAM does not was ascribed to the fact that one end of the amide dipole ($N^{\delta+}$-) is part of the polymer main chain in the case of PiPrOx, whereas in PNIPAM the entire dipolar unit is part of the side chain. There is no strong experimental evidence so far that PiPrOx chains are partially organized in cold aqueous solutions below the LCST. However, Chen et al. have demonstrated by static and dynamic light scattering that poly(2-ethyl-2-oxazolines) (PEtOx) in water experience partial organization and large-scale concentration fluctuations at all temperatures, even well below the LCST.[36] This organization was ascribed to a special orientation between polymer molecules, triggered by dipolar interactions between amide fragments. Such partial organization in cold water may lead to preferential orientations of the polymer chains in the coagulates and, in the case of PiPrOx, promote crystallization of the polymer.

Having on hand a series of telechelic and semitelechelic HM-PiPrOx of various molecular weights, C_{18}-PiPrOx-C_{18} and C_{18}-PiPrOx-OH, respectively (Figure 2),[19] we set about to assess the impact of end-group modification on the heat-induced phase separation and crystallization of PiPrOx in water. The results of this study are reported here. We examine first the mechanistic aspects of the heat-triggered association by analysis of the thermodynamic parameters of the phase transition of the micellar solutions. To evaluate them, we employed HS-DSC, pressure perturbation calorimetry (PPC), and turbidimetry, taking care to employ conditions adjusted to prevent, or minimize, crystallization of PiPrOx. In a second part we subjected micellar polymer solution to prolonged heating above the phase transition temperature in order to induce crystallization of the polymer. The materials obtained by this treatment were analyzed by X-ray diffraction and differential scanning calorimetry. They were also

Table 1. Physical Properties of the Polymers Investigated[a]

polymer	M_n[b]	M_w/M_n[b]	n[c]	R_H[d]
Me-PiPrOx-OH 6K	*5700*[e]	*1.03*[e]	*50*[e]	
Me-PiPrOx-OH 10K	10400	1.06	90	
C_{18}-PiPrOx-OH 7K	6700	1.21	57	7.2 ± 0.5
C_{18}-PiPrOx-OH 10K	9900	1.17	85	8.2 ± 0.8
C_{18}-PiPrOx-OH 13K	12800	1.16	111	2.9 ± 0.3
C_{18}-PiPrOx-C_{18} 7K	7000	1.15	57	7.6 ± 0.4
C_{18}-PiPrOx-C_{18} 10K	10300	1.15	85	10.5 ± 0.3[f]
				126 ± 0.7[f]
C_{18}-PiPrOx-C_{18} 13K	13100	1.18	111	7.9 ± 0.5[f]
				102 ± 0.4[f]

[a] From ref 19. [b] M_n and M_w: number- and weight-average molecular weight from GPC analysis. [c] Number of monomer units per chain. [d] R_H: hydrodynamic radius of HM-PiPrOx micelles in water, from dynamic light scattering measurements. [e] Values given in italics are taken from ref 27. [f] Bimodal size distribution.

observed by polarized optical microscopy and transmission electron microscopy. One outcome of this study is that it provides experimental evidence that the structure, conformation, and alignment of the polymer main chain can induce phase changes within the inner hydrophobic core of the flower micelles, an effect which has not been observed previously. Another important observation is that while semitelechelic HM-PiPrOx samples crystallize from hot water, telechelic HM-PiPrOx samples do not crystallize under these conditions. The resistance against crystallization from hot water of telechelic HM-PiPrOx may be taken as an indication that the memory of the flowerlike self-assembled structures of the telechelic polymers in cold water is retained in the aggregates formed in solutions heated above their phase-transition temperature.[37]

Experimental Section

Materials. Water was deionized with a Millipore Milli-Q system. Deuterium oxide (99.8%) was purchased from Aldrich-Sigma Chemicals. The semitelechelic and telechelic HM-PiPrOx samples were prepared and characterized as described previously.[19] All semitelechelic HM-PiPrOxs readily dissolved in water. However, telechelic HM-PiPrOxs recovered after precipitation were only soluble in water up to a concentration of ~2.0 g L^{-1}. In order to enhance their solubility in water, the polymers were dissolved in dimethyl sulfoxide (DMSO, 5.0 g L^{-1}) and dialyzed against water for 3 days using membranes of MWCO 1000 g mol^{-1}. The polymers recovered by lyophilization of the dialysates dissolved readily in water up to a concentration of 20 g L^{-1}. Their molecular characteristics are listed in Table 1. The sample of unmodified PiPrOx used in control experiments (Me-PiPrOx-OH 10K, $M_n = 10\,400$ g mol^{-1}, PDI = 1.06) was obtained by cationic ring-opening polymerization using methyl *p*-tosylate as initiator, as described elsewhere.[27]

Transmittance Measurements. Cloud points were determined by spectrophotometric detection of the changes in turbidity ($\lambda = 550$ nm) of aqueous polymer solutions (0.1−10 g L^{-1}) heated at a constant rate (1 °C min^{-1}). The values reported are the temperatures corresponding to a 20% decrease of the solution transmittance. The estimated error in T_{cp} determined by this procedure is ±0.5 °C.

High-Sensitivity Differential Scanning Calorimetry (HS-DSC). HS-DSC measurements were performed on a VP-DSC microcalorimeter (MicroCal Inc.) at an external pressure of ca. 180 kPa. The cell volume was 0.517 mL. The heating rate was 0.3 °C min^{-1}. Polymer solutions, ranging in concentration from 0.1 to 10 g L^{-1}, were degassed at 25 °C for 20 min. They were equilibrated at 10 °C for 1 h before initiation of the heating process. For each measurement, the sample was heated from 10 to 80 °C and cooled back immediately to 10 °C, unless stated otherwise. Four consecutive scans were performed; a small (<10%) decrease of the transition enthalpy was detected after four scans. To assess the effect of prolonged sample heating on the DSC traces, a solution of C_{18}-PiPrOx-OH 10K (1.0 g L^{-1}) was subjected to six consecutive heating/cooling scans at a constant rate (0.3 °C min^{-1}) separated by 1 h incubation at 80 and 10 °C. The transition enthalpies recorded for successive scans decreased progressively (Figure SI.1), an indication of a gradual change in the concentration of polymer soluble in cold water due to its irreversible crystallization when incubated in the calorimeter cell at 80 °C. Data were corrected for instrument response time to take into account the effect of scan rate on the data collected. For each solution, the excess heat capacity curve was constructed by subtraction of a water vs water scan from the sample vs water scan. The difference in heat capacity after and before transition (Δc_p) was calculated from the position of the baseline before and after the phase transition (see inset in Figure 3).

Data were fitted with two models using software supplied by the manufacturer. A cubic connect baseline was subtracted from the data prior to fitting. A two-state transition model was applied first. It generated T_M and the enthalpy change ΔH. A non-two-state transition model, which was proposed by Tanaka et al. to describe protein unfolding,[38] was used to fit the data when fits with the two-state model were poor. This model allows one to determine (i) the calorimetric heat (ΔH) from the area under a transition peak and (ii) the van't Hoff heat ΔH_{vH} based on the shape of the transition peak. Experimental data acquired for solutions of telechelic and semitelechelic PiPrOx 10K (squares) together with the fit curves using a non-two-state model are shown in Figure 3. The total molar heat capacity of the system $c_p(T)$ is given by eq 1:

$$c_p(T) = \frac{K_{Lo}(T)\Delta H_{Lo,vH}\Delta H_{Lo}}{(1+K_{Lo}(T))^2 RT^2} + \frac{K_{Hi}(T)\Delta H_{Hi,vH}\Delta H_{Hi}}{(1+K_{Hi}(T))^2 RT^2} \quad (1)$$

where $K_{Lo}(T)$ and $K_{Hi}(T)$ are the equilibrium constants for the lower and higher temperature phase transition, respectively, ΔH_{Lo} and ΔH_{Hi} are the molar enthalpy changes for the low and high temperature transitions, respectively, $\Delta H_{Lo,vH}$ and $\Delta H_{Hi,vH}$ are the van't Hoff heat changes for the low and high temperature transitions, respectively, R is the gas constant, and T is the temperature.

The equilibrium constants were evaluated for each transition using eqs 2 and 3:

$$K_{Lo}(T) = \exp\left\{\frac{-\Delta H_{Lo,vH}}{RT}\left(1 - \frac{T}{T_{Lo}}\right)\right\} \quad (2)$$

$$K_{Hi}(T) = \exp\left\{\frac{-\Delta H_{Hi,vH}}{RT}\left(1 - \frac{T}{T_{Hi}}\right)\right\} \quad (3)$$

where T_{Lo} and T_{Hi} are the lower and higher transition temperatures, respectively. Equations 1, 2, and 3 are then used for curve-fitting in the usual way yielding the set of parameters: T_{Lo}, T_{Hi}, ΔH_{Lo}, ΔH_{Hi}, $\Delta H_{Lo,vH}$, and $\Delta H_{Hi,vH}$. The estimated error in ΔH determined by this procedure is ±0.05 kJ mol^{-1}.

Pressure Perturbation Calorimetry (PPC). PPC measurements were performed on a VP-DSC microcalorimeter equipped with a pressure perturbation accessory (MicroCal Inc.). The gas (N_2) pressure jump applied to the samples was 500 kPa. The reference cell and sample cell volumes were identical (0.517 mL). The concentration of the solutions analyzed was 2.5 g L^{-1}. Under the same experimental conditions, a set of reference measurements was carried out each time. A detailed description of the method has been reported elsewhere.[39,40] In a differential calorimetric experiment, the sample and reference cells are filled respectively with a solute (polymer in our measurements) solution and with solvent. When both cells are subjected to the same

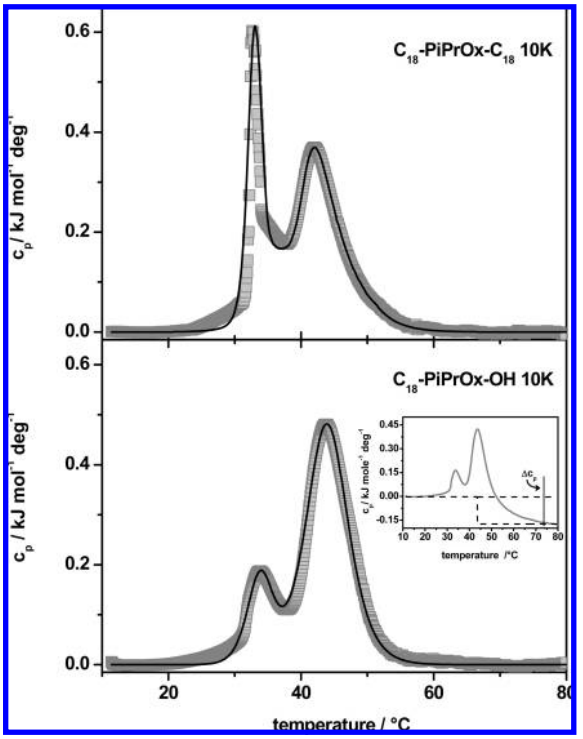

Figure 3. Microcalorimetric endotherms (heating rate: 0.3 °C min^{-1}) recorded for solutions of telechelic (top) and semitelechelic (bottom) PiPrOx 10K (polymer concentration: 1.0 g L^{-1}). DSC data were fitted using a non-two-state model for two transitions (see text).

pressure change ΔP, the thermal expansion coefficient, α, of the solute can be calculated from eq 4:

$$\alpha = \alpha_s - \frac{\Delta Q}{T \Delta P m_p \overline{V}_p} \tag{4}$$

where α_s is the thermal expansion coefficient of the solvent, T is the temperature, m_p and $\overline{V}_P$ are the polymer mass and partial specific volume in the solution, respectively, and ΔQ is the net heat (i.e., the difference between sample cell and the reference cell, which contain solvent only). The value of partial specific volume of PiPrOx[27] used for volumetric calculations was $\overline{V}_P = 0.888$ cm^3 g^{-1}. The same value of $\overline{V}_P$ was used for the hydrophobically modified HM-PiPrOx samples.

The volume change ΔV, which accompanies transitions in the system, was obtained from the area under the curves by fitting the data using the non-two-state transition model, as indicated in eqs 5 and 6, where we assume that ΔV is small compared to V. The value ΔV is expressed as a percent of V.

$$\frac{\Delta V^{Lo}}{V} = \int \alpha^{Lo}\, dT = \int \frac{1}{V}\left(\frac{dV}{dT}\right)^{Lo} dT \tag{5}$$

$$\frac{\Delta V^{Hi}}{V} = \int \alpha^{Hi}\, dT = \int \frac{1}{V}\left(\frac{dV}{dT}\right)^{Hi} dT \tag{6}$$

where the superscripts "Lo" and "Hi" denote changes occurring during T_{Lo} and T_{Hi} transitions, respectively.

Crystallization Studies. Aqueous solutions of Me-PiPrOx-OH 10K and HM-PiPrOxs (10 g L^{-1}) were prepared by dissolving each polymer in water and gentle stirring at room temperature for at least 12 h. They were heated in an oil bath kept at 70 °C for 24 h. They were cooled and subjected to freeze-drying to yield a white solid, which was used directly for XRD and TEM analysis.

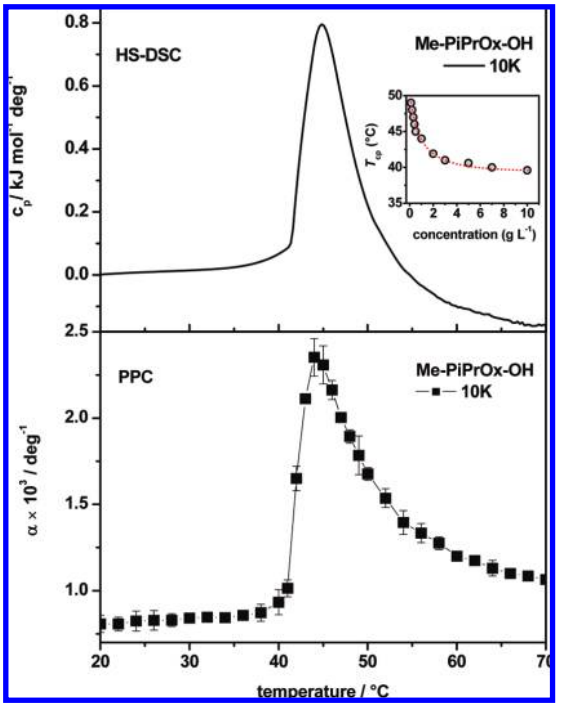

Figure 4. (top) Microcalorimetric endotherm (polymer concentration: 1.0 g L^{-1}) and (bottom) temperature dependence of the coefficient of thermal expansion (α) of an aqueous solution of Me-PiPrOx-OH 10K (polymer concentration: 2.5 g L^{-1}).

Transmission Electron Microscopy (TEM). TEM imaging was performed with a FEI Tecnai 12 microscope operated at 120 kV. The powders recovered by freeze-drying the solutions employed for the heat treatment (at 70 °C for 24 h), as noted above, were redispersed in a small amount of water and placed on carbon-coated Cu grids (1 drop of ~10 μL). The water was evaporated at room temperature. The samples were negatively stained with phosphotungstic acid (0.5 wt % in water) prior to observation.

X-ray Diffraction (XRD). XRD studies were carried out with a Bruker diffractometer (D8 Discover), using Cu Kα radiation (λ=1.542 Å). The diffraction pattern was recorded with a Bruker AXS two-dimensional wire-grid detector. Polymer samples (Me-PiPrOx-OH 10K, HM-PiPrOxs 7K and 10K), prepared from the residues obtained after freeze-drying the solutions employed for the heat treatment (at 70 °C for 24 h) as noted above, were packed into 1.0 mm diameter capillary tubes (Charles Supper). 1-D data were obtained by integrating the 2-D data. The *d*-spacings were determined from the maximum of the diffraction peaks according to the Bragg equation, $n\lambda = 2d \sin\theta$, where n is an integer giving the order of the diffraction peak, θ is the angle of incidence, and λ is the wavelength of the X-ray beam used.

Results and Discussion

Temperature-Dependent Properties of Aqueous Me-PiPrOx-OH Solutions. We present first salient features of the heat-induced phase transition of dilute aqueous solutions of an unmodified polymer, Me-PiPrOx-OH 10K, that has a molecular weight within the range of the HM-PiPrOx samples examined here (see Table 1). The cloud point (T_{cp}) of aqueous Me-PiPrOx-OH 10K, obtained by turbidity measurements, decreases with increasing concentration from ~48 °C (c = 0.1 g L^{-1}) to ~39 °C (c = 10 g L^{-1}) (Figure 4, inset), in agreement with previous reports.[27] Microcalorimetry scans recorded for aqueous solutions of Me-PiPrOx-OH 10K (1.0 g L^{-1}) feature a broad, markedly asymmetric endotherm, with a sharp increase of the heat capacity on

Table 2. Thermal Properties of Various Semi- and Telechelic HM-PiPrOx Aqueous Solutions (Polymer Concentration 1.0 g L^{-1})[a]

			ΔH_{Lo} (kJ mol^{-1})		$\Delta H_{Lo,\ vH}$ (kJ mol^{-1})		ΔH_{Hi} (kJ mol^{-1})	$\Delta H_{Hi,vH}$ (kJ mol^{-1})
polymer	T_{cp} (°C)	T_{Lo} (°C)	iPrOx unit	C_{18} unit	iPrOx unit	T_{Hi} (°C)	iPrOx unit	iPrOx unit
Me-PiPrOx-OH 6K	48.1[b]					48.0[b]	5.65[b]	
						47.0	*5.98*	
Me-PiPrOx-OH 10K	44.0					44.8	5.75	460
						43.4	*5.90*	*525*
C_{18}-PiPrOx-OH 7K	32.5	32.7	1.35	77	515	46.8	1.90	240
		32.6	*1.42*	*81*	*640*	*45.7*	*2.15*	*290*
C_{18}-PiPrOx-OH 10K	33.2	34	0.98	83	525	43.5	4.15	395
		33.7	*0.85*	*73*	*600*	*42.3*	*4.25*	*445*
C_{18}-PiPrOx-OH 13K	39.0					41.5	5.60	605
						40.8	6.05	650
C_{18}-PiPrOx-C_{18} 7K	31.6	31.5	1.91	55	500	46.3	1.84	290
		32.0	*1.70*	*49*	*680*	*45.2*	*2.00*	*315*
C_{18}-PiPrOx-C_{18} 10K	32.1	32.6	1.30	56	1100	42.1	3.30	360
		32.8	*1.22*	*52*	*1200*	*41.2*	*3.55*	*375*
C_{18}-PiPrOx-C_{18} 13K	34.9	34.4	1.42	79	1400	40.7	3.70	310
		34.5	*1.32*	*75*	*1500*	*39.9*	*4.05*	*340*

[a] Measurements were done in H_2O and D_2O; values given in italics are obtained for solutions in D_2O. [b] Values taken from ref 27.

the low-temperature side and a gradual decrease of the heat capacity for temperatures higher than the maximum transition temperature (T_M) (Figure 4, top). The temperature corresponding to the onset of the endotherm (T_{onset}) is nearly identical to the solution cloud point obtained by turbidimetry,[26] an indication that the heat-induced solution turbidity is coupled to the dehydration of the polymer chains and their subsequent aggregation. Beyond the phase transition temperature, the solution heat capacity levels off toward a value significantly lower than the initial value ($\Delta c_p \sim -180$ J mol^{-1} C^{-1}). A similar trend was reported for aqueous solutions of PNIPAM 10K ($\Delta c_p \sim -107$ J mol^{-1} C^{-1}),[22] poly(vinylcaprolactam) ($\Delta c_p \sim -70$ J mol^{-1} C^{-1}),[41] and various pluronic-type block copolymers.[42] It is usually taken as an indication of diminished interactions between water molecules and polymer chains in solutions heated beyond their phase transition temperature. The T_M value depends on the molecular weight of the sample, and for a given polymer, it decreases with polymer concentration (0.1−10 g L^{-1}).[27] Thermograms were recorded also with solutions of Me-PiPrOx-OH 10K in D_2O, in order to assess the relative importance of solvent/polymer and polymer/polymer interactions. The transition enthalpy was higher for solutions in D_2O, compared to solutions in H_2O. This trend, which is commonly observed for the phase transition of polymers in aqueous solutions, reflects the fact that a "hydrogen" bond in D_2O is about 5% stronger than a hydrogen bond in H_2O.[43] The T_M value recorded for the solution in D_2O is lower, by ~1.5 °C, than that obtained in H_2O. In general, D_2O promotes processes that tend to reduce the accessible apolar surface area (ASA_{ap}), such as micelle formation,[44] protein folding,[45] or the fluid-to-gel phase transition of lipids.[46]

The simplest analysis of the HS-DSC data, which assumes a two-state transition, did not lead to a satisfactory fit of the data. However, analysis of the data using a non-two-state model[38] yielded an acceptable fit, with a van't Hoff enthalpy change (ΔH_{vH}) of ~460 kJ mol^{-1}, along with a calorimetric enthalpy change (ΔH) of ~5.7 kJ mol^{-1} (Table 2). The relative magnitudes of ΔH and ΔH_{vH} are gauges of the cooperativity of the transition, as described previously in studies of PNIPAM and poly(*N*-*n*-propylacrylamide).[47] Since the calorimetric heat refers to the enthalpy change *per mole of iPrOx unit*, whereas the van't Hoff enthalpy is the heat change per polymer segment involved as a whole in the transition, the ratio $\Delta H_{vH}/\Delta H$ gives an estimate of the number of units undergoing cooperative phase transition. In the terminology used to describe protein unfolding, the coil-to-globule transition of Me-PiPrOx-OH occurs by a mechanism involving independent domains ~80 iPrOx units in length or of $M_n \sim 10\,400$ g mol^{-1}. Consequently, for a PiPrOx of $M_n \sim 10\,000$ g mol^{-1} the transition can be regarded as an "all or none" process. A similar conclusion was reached by Tiktopulo et al.[48] in their study of the phase transition of aqueous PNIPAM for which the number of repeat units per domain was ~90 ($M_n \sim 11\,200-370\,000$ g mol^{-1}).

Information on the changes in the hydration layer around the polymer chain as it undergoes coil-to-globule collapse was obtained by pressure perturbation calorimetry (PPC). A PPC scan recorded for a solution of Me-PiPrOx-OH 10K (2.5 g L^{-1}) is presented in Figure 4, bottom. The thermal expansion coefficient, α, is constant for $T < T_{onset}$; after this point it increases sharply with increasing temperature, passes through a maximum value at $T \sim 44$ °C, and gradually decreases as the temperature increases further. It is interesting to note that the PPC and DSC transition peaks have the same shape. This confirms that the changes in volume and in enthalpy occurring during the transition are coupled.[49] Similar results have been reported in studies of micellar sphere-to-rod transitions,[50] of the chain melting transitions of phospholipids,[51] and the LCST transition of PNIPAM.[39] Integration of the changes of $\alpha(T)$ vs T yields ΔV, the change in the hydration volume of the polymer as the solution undergoes the phase transition, assuming that the intrinsic volume of the polymer does not change. The percent change of the partial volume of the polymer, $\Delta V/V$, is 1.5% for Me-PiPrOx-OH 10K (Table 3), a value significantly higher than the value recorded for PNIPAM (1.0%).[39] This relatively large change, compared to PNIPAM, indicates that the volume of the water released during the transition is larger in the case of Me-PiPrOx-OH or/and that the volume occupied by PiPrOx chains in the separated phase is smaller, possibly as a consequence of the existence of interchain associations via dipolar interactions noted in previous studies of polyoxazolines.[36]

Litt et al.[52] established in the early 1970s that PiPrOx is a semicrystalline polymer. Its X-ray diffractogram presents an equatorial reflection (assigned to the 010 plane) with a *d*-spacing = 10.9 Å, a value attributed to the distance between the backbone of adjacent chains, and a periodicity along chain of 6.4 Å. We confirmed the crystallinity of Me-PiPrOx-OH-10K by polarized optical microscopy (Figure SI.2) and DSC. The polymer melts at 201 °C and has a T_g of ~66 °C (see Figure SI.3). We assessed also the ability of Me-PiPrOx-OH 10K to crystallize from hot water.[35] An aqueous

Table 3. Thermodynamic Characteristics of Aqueous Polymer Solutions by Pressure Perturbation Calorimetry (Polymer Concentration 2.5 g L^{-1})

polymer	T_{Lo} (°C)	$\Delta V/V^{Lo}$ (%) (°C)	T_{Hi} (°C)	$\Delta V/V^{Hi}$ (°C) (%)	$\Delta V/V^{T}$ [a] (%)
Me-PiPrOx-OH 10K			44.0		1.52
Me-PiPrOx-OH 6K			*45.0*[b]		*1.10*[b]
C_{18}-PiPrOx-OH 7K	33.8	0.39 (40%[c])	46.2	0.57	0.96
C_{18}-PiPrOx-OH 10K	35.0	0.11 (7%[c])	43.0	1.40	1.51
C_{18}-PiPrOx-OH 13K			42.0	1.38	1.38
C_{18}-PiPrOx-C_{18} 7K	34.0	0.38 (42%[c])	44.0	0.51	0.90
C_{18}-PiPrOx-C_{18} 10K	35.5	0.20 (15%[c])	42.0	1.11	1.31
C_{18}-PiPrOx-C_{18} 13K	36.0	0.25 (17%[c])	40.0	1.20	1.45

[a] Total value of $\Delta V/V$. [b] Values given in italics are taken from ref 27. [c] Fraction of the low-temperature volume change ($\Delta V/V^{Lo}$) contributing to the total volume change ($\Delta V/V^{T}$).

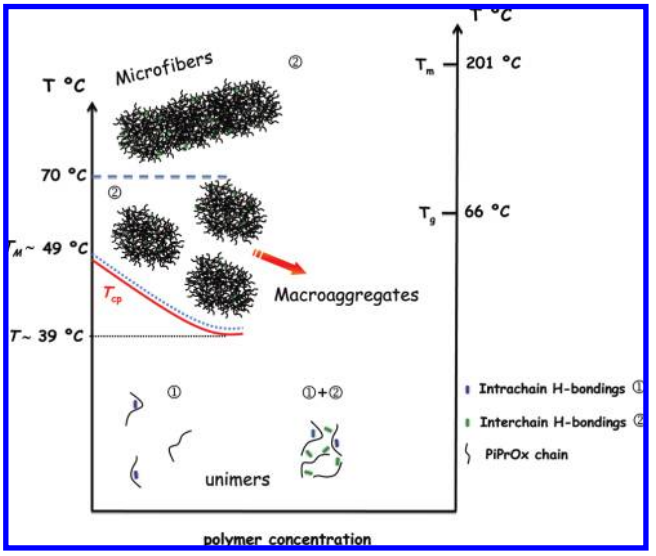

Figure 5. Temperature−concentration phase diagram of Me-PiPrOx-OH 10K/water system. It pictorially shows cloud point (red) and collapse transition (dotted blue) lines which correspond to the dehydration and aggregation of polymer chains in the form of macroaggregates and eventually microfibers. The crystallization domain (blue dashed line) observed here was previously reported (ref 35). T_m and T_g values were determined by DSC measurements.

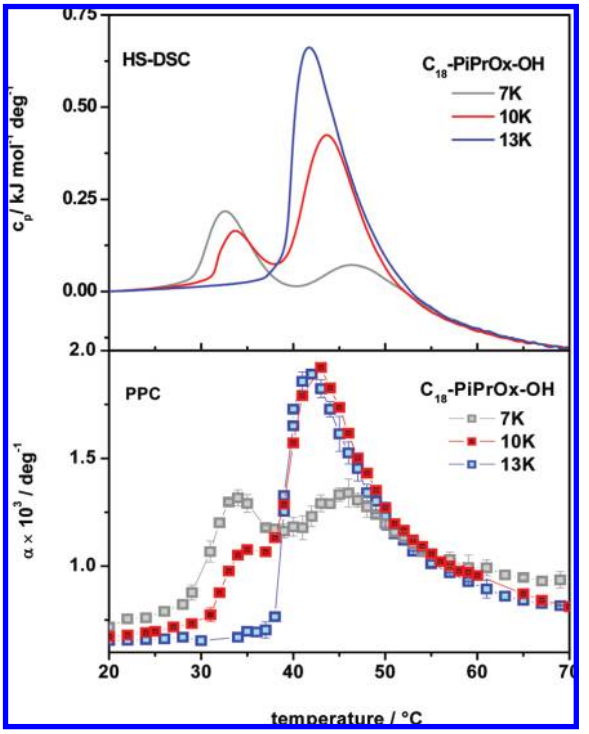

Figure 6. (top) Microcalorimetric endotherms (polymer concentration: 1.0 g L^{-1}) and (bottom) temperature dependence of the coefficient of thermal expansion (α) (polymer concentration: 2.5 g L^{-1}) of aqueous solutions of C_{18}-PiPrOx-OH.

solution (10 g L^{-1}) of Me-PiPrOx-OH 10K was heated past its cloud point and kept at 70 °C for 24 h. Upon cooling to room temperature, the mixture did not recover its clarity but formed a soft white gel. The dry powder isolated by lyophilization of the gel displayed an XRD pattern characteristic of PiPrOx.

Data gathered from the complete study of aqueous Me-PiPrOx-OH 10K are represented pictorially in the phase diagram of the polymer/water system (Figure 5), in which we represent (a) the cloud point line obtained from turbidimetry measurements, (b) the collapse transition line, from HS-DSC scans, which corresponds to the dehydration and aggregation of the polymer in the form of macroaggregates, and (c) the bulk melting temperature (T_m) and the glass transition temperature (T_g) measured by DSC of bulk polymer.

Temperature-Dependent Properties of Aqueous C_{18}-PiPrOx-OH Solutions. Previous studies based on DLS and SAXS measurements revealed that the semitelechelic samples C_{18}-PiPrOx-OH 7K and C_{18}-PiPrOx-OH 10K self-assemble in cold water to form star micelles ($R_H \sim 8$ nm) consisting of a hydrophobic core ($R_c \sim 1.3$ nm) surrounded by a corona of dangling PiPrOx chains, while the polymer of highest molecular weight, C_{18}-PiPrOx-OH 13K, is molecularly dissolved in cold water without detectable micellization.[19] The solution cloud point of the three semitelechelic HM-PiPrOx-OH is lower than that of the unmodified Me-PiPrOx-OH 10K (Table 2). The T_{cp} depression upon end-group modification is the largest (~12 °C) in the case of the shortest polymer (C_{18}-PiPrOx-OH 7K). The T_{cp} values of aqueous C_{18}-PiPrOx-OH 10K solutions decrease from 34.5 to 33 °C with increasing polymer concentration (from 0.1 to 10 g L^{-1}; see Figure 7, inset). We know from DLS measurements that the enhanced turbidity of C_{18}-PiPrOx-OH 7K and C_{18}-PiPrOx-OH 10K aqueous solutions heated past their cloud point temperature reflects the formation of large objects ($R_H \sim 400-700$ nm) which slightly decrease in size ($R_H \sim 250$ nm) as the temperature exceeds 45 °C.[19]

HS-DSC and PPC traces of the three semitelechelic PiPrOxs (M_n = 7K, 10K, and 13K) are presented in Figure 6. Unexpectedly, the $c_p(T)$ vs T and $\alpha(T)$ vs T curves recorded for solutions of C_{18}-PiPrOx-OH 7K and C_{18}-PiPrOx-OH 10K present two maxima for temperatures denoted T_{Lo} and T_{Hi}. We took great care to ascertain that none of the two endotherms were due to some artifact. Trivial causes, such as contamination of the polymers, of the solutions, or of the microcalorimeter cells, were dismissed after careful purifications and control measurements using several microcalorimeters. Furthermore, we monitored the effect of the heating

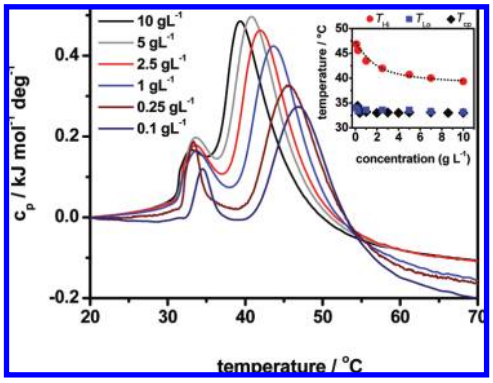

Figure 7. Microcalorimetric endotherms recorded for aqueous solutions of C_{18}-PiPrOx-OH 10K of polymer concentration ranging from 0.1 to 10 g L^{-1}.

rate and found that, within experimental uncertainty, the position of T_{Hi} was not affected, while the T_{Lo} value increased by no more than 0.5 °C as the heating rate was raised from 0.3 to 1.5 °C min^{-1} (Figure SI.4). We monitored the effect of polymer concentration (from 0.1 to 10 g L^{-1}) on the position of the two maxima, as shown in Figure 7 in the case of aqueous C_{18}-PiPrOx-OH 10K solutions. The value T_{Hi} showed a marked concentration dependence, decreasing with increasing concentration, whereas T_{Lo} was hardly affected by changes in concentration. Moreover, the T_{Lo} values are nearly identical to the T_{cp} values determined by turbidimetry (Figure 7, inset). In Figure 6 (blue curve), we present also the thermogram recorded for a solution of the longest semitelechelic HM-PiPrOx (C_{18}-PiPrOx-OH 13K, 1.0 g L^{-1}). It features a single endotherm, and the thermodynamic parameters associated with the phase transition of this polymer are similar to those of the unmodified Me-PiPrOx-OH 10K (Table 2).

To unveil the molecular origin of each transition, we scrutinized how the molecular weight of the polymer affects each parameter extracted from the HS-DSC data listed in Table 2. For the transition taking place at higher temperature, we observed the following trends: (i) The temperature of the transition (T_{Hi}) decreases with increasing polymer molecular weight, a characteristic feature of the PiPrOx chain.[27] (ii) The calorimetric enthalpy (ΔH_{Hi}) for C_{18}-PiPrOx-OH 7K and C_{18}-PiPrOx-OH 10K is lower than the value registered for the phase separation of the unmodified PiPrOx. Since the heat evolved in the process is attributable to the release of water molecules bound to the polymer chains into bulk water, it can be inferred from the ΔH_{Hi} values that fewer polymer/water bonds are broken, per iPrOx unit, during the heat induced phase transition of the semitelechelic HM-PiPrOx solutions, compared to homopolymer solutions. The difference is particularly large for the shortest polymer, whereas the ΔH value recorded for solutions of the longest polymer C_{18}-PiPrOx-OH-13K, which does not micellize, is identical to the value recorded for solutions of unmodified PiPrOx (Table 2). The trend can be taken as an indication that near the core of the star micelles the polymer chains are crowded to such an extent that the monomer density is sufficiently high to prevent, or hinder, the formation of water/polymer hydrogen bonds, as reported earlier in the case of HM-PNIPAM samples.[53] (iii) The van't Hoff heat ($\Delta H_{Hi,vH}$) also increases with the molecular weight of the semitelechelic HM-PiPrOx (Table 2). The number of cooperative units determined based on the enthalpy values obtained for the T_{Hi} transitions (90 ± 10) are of the same order as the unmodified polymers, which implies that more than one polymer chain may be involved cooperatively in the case of C_{18}-PiPrOx-OH 7K. (iv) The largest contribution to $\Delta V/V$, from 60 to 90% of the total value (Table 3), arises from the transition centered around T_{Hi}. Recalling that the magnitude of $\Delta V/V$ is related to the change in the hydration volume of the polymer chain, it can be concluded that most of the water of hydration bound to the polymer micelles is released into bulk during the transition centered around T_{Hi}. (v) The T_{Hi} measured with polymer solutions in D_2O is consistently lower (by ~1 °C), compared to the value recorded for solutions of the polymers in H_2O. Taken together, the thermodynamic information gathered for the endotherm centered at T_{Hi} carries the typical signature of the dehydration of the PiPrOx chain that accompanies the LCST phase transition.

Turning our attention now to the lower temperature endotherm, we note that the T_{Lo} values are nearly identical to the cloud points of the corresponding solutions and that, like T_{cp}, they increase with increasing polymer molecular weight and are nearly independent of polymer concentration (see inset Figure 7). Therefore, this endotherm must be related to the formation of clusters of micelles, which is responsible also for the increase in solution turbidity, rather than to the dehydration of the PiPrOx chain. Ancillary support for this hypothesis is provided by the fact that the thermogram recorded for a solution of the polymer C_{18}-PiPrOx-OH-13K, which does not micellize in water, features only one transition closer in temperature to T_{Hi} then to T_{Lo} (Figure 6). It also appears that the transition around T_{Lo} involves fewer changes in polymer/water interactions than the transition around T_{Hi}, since the T_{Lo} and ΔH_{Lo} values recorded for solutions of the polymers in D_2O and in H_2O are nearly identical. We calculated the ΔH_{Lo} of the transition per mole of *n*-octadecyl group, rather than per monomer unit (see Table 2 in which the enthalpy is reported in both units). This enthalpy is the same for both polymers. Its value (~80 kJ/mol $C_{18}H_{37}$) is on the same order of magnitude as the enthalpy of fusion of *n*-octadecane (61 kJ mol^{-1}).[54]

Taking into consideration all the information collected so far, we propose the following interpretation for the two phase transitions observed in solutions of semitelechelic HM-PiPrOx star micelles (see Figure 8 for a pictorial representation). Considering first the structure of the star micelles, one needs to remember that the PiPrOx chains are kept in a rigid extended conformation as a consequence of the presence of the amide nitrogens in the main chain. When placed in close proximity, the PiPrOx chains tend to align through the amide dipoles. This reduces the degree of freedom of the end alkyl chains confined in the micelle core. In the concentration regime of interest here, polymer micelles in solution are brought into contact as a consequence of thermal concentration fluctuations. As the temperature increases, intermicellar contacts become more frequent. Permanent polymer/polymer contacts are formed, possibly via H-bond with a water molecule acting as cross-linker.[55] These events affect the core of the micelles, allowing the hydrophobic groups to gain additional degree of freedom, such that the core of the micelle undergoes a phase transition ("melting") from a rigid phase to a more fluid one. This transition can be associated with the endotherm centered at T_{Lo}, a temperature in the vicinity of the melting point of *n*-octadecane (28−30 °C).[54] Rearrangement of the micellar core may be accompanied by core merging and formation of elongated ("rodlike") micelles. Heerklotz et al. reported that structural sphere-to-rod transitions of detergent micelles are accompanied by volume changes detected by PPC.[50] Similarly,

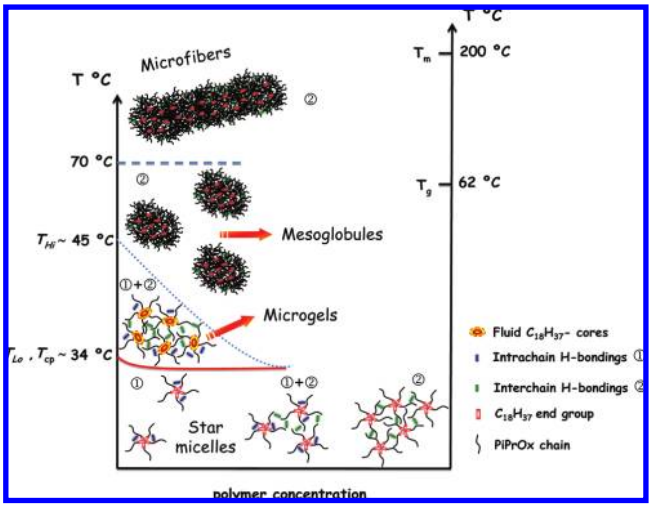

Figure 8. Temperature−concentration phase diagram of C_{18}-PiPrOx-OH 10K/water system. It pictorially shows cloud point (red) and collapse transition (blue) lines which correspond to the aggregation and dehydration of the polymer, respectively, together with associated structures such as microgels and aggregates of mesoglobules and the crystallization domain (blue dashed line).

the PPC signal associated with the low-temperature transition (Figure 6 and Table 2) may be due to a star-to-rod transition in the case of the semitelechelic samples. Preliminary results from temperature-dependent SAXS studies of semitelechelic HM-PiPrOx in water suggest the formation of cylindrical objects for solutions heated to a temperature in the vicinity of T_{Lo}.[56] Assembly of numerous rodlike micelles, via H_2O-mediated cross-linking of PiPrOx chains, results in the formation of microgel particles (a few micrometers in diameter) in which the PiPrOx are still hydrated. As the solution temperature reaches the LCST of PiPrOx, dehydration of the chains occurs. It is responsible for the T_{Hi} transition.

There are previous reports of two well-separated heat-induced phase transitions in systems involving thermosensitive polymers. For example, Shan et al. found that high-density PNIPAM brushes grafted onto gold nanoparticles undergo a first transition around 31 °C and a second one around 35 °C.[57] They attributed the low-temperature transition to the dehydration of the inner regime of the PNIPAM brush, while the high-temperature transition was assigned to the outer, less dense regime, of the PNIPAM brush. Similar phenomena were reported in the case of dense PNIPAM brushes grafted to the surface of a hyperbranched polyester hydrophobic core.[58] In both cases, the phenomenon is a consequence of the properties of short, dense PNIPAM brushes. One may argue that the coronae of the C_{18}-PiPrOx-OH 7K and C_{18}-PiPrOx-OH 10K star micelles may be regarded as polymer brushes and that the two transitions observed here have the same mechanistic origin. Several characteristics of the HM-PiPrOx phase transitions are difficult to rationalize from the viewpoint of polymer brushes physics. In particular, this interpretation does not account for the fact that the first transition (T_{Lo}), assigned in the case of PNIPAM-grafted gold nanoparticles to the dehydration of the inner brush, is concomitant, in our case, with the aggregation of star micelles into micrometer-sized objects. Moreover, it explains neither the lack of isotope effect (H_2O vs D_2O) during the T_{Lo} transition nor the fact that ΔH_{Lo} correlates with the concentration of *n*-octadecyl chains but not with the concentration of iPrOx units.

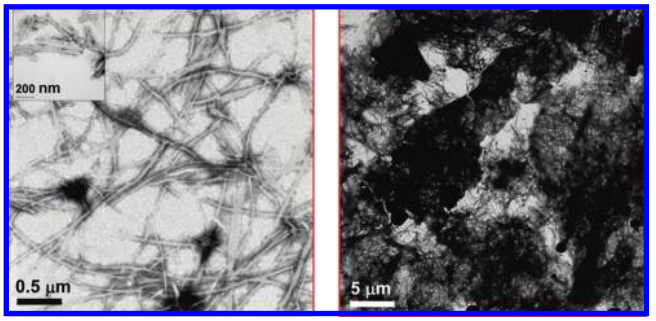

Figure 9. Transmission electron microscopy images of microfibers obtained after (left) 5 h and (right) 24 h heat treatments at 70 °C of an aqueous solution of C_{18}-PiPrOx-OH 10K (10 g L^{-1}).

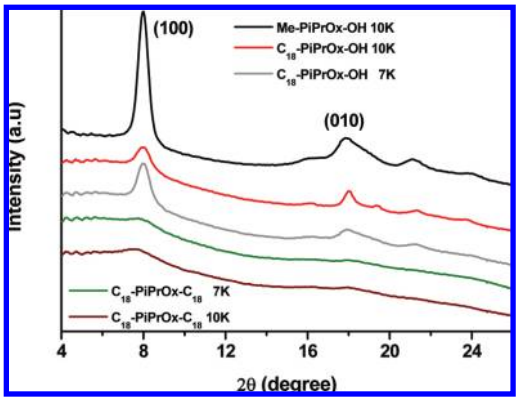

Figure 10. XRD data of dried Me-PiPrOx-OH 10 K and HM-PiPrOxs coagulates formed in water at 70 °C.

We were intrigued to know if the presence of hydrophobic domains would prevent the crystallization of the PiPrOx chain in the collapsed microgels formed for $T > T_{Hi}$. Thus, semitelechelic HM-PiPrOx samples were incubated at 70 °C for 5 and 24 h. Upon cooling soft white gels were recovered, as in the case of the unmodified polymer. Transmission electron microscopy images of gels obtained after 5 and 24 h heat treatments are presented in Figure 9. Specimens recovered after 5 h form long interconnected fibers ~40 nm in diameter. With increasing heating time, the fibers assemble in large bundles that create an extensive network, presumably responsible for the macroscopic gelation of the fluid. The heat-treated samples were characterized also by X-ray diffraction measurements performed on the powders recovered by lyophilization. The diffractograms (Figure 10) of the semitelechelic HM-PiPrOx powders present two major peaks, at $2\theta = 8.15°$ ($d = 10.8$ Å) and $2\theta = 17.2°$ ($d = 5.16$ Å), also featured in the XRD trace of a heat-treated Me-PiPrOx-OH sample and in agreement with the report of Litt et al.[52] These experimental data lead us to conclude that semitelechelic HM-PiPrOx samples crystallize from hot water, allowing us to complete the phase diagram of the system semitelechelic HM-PiPrOx/water in the case of polymers able to form star micelles in cold water, e.g., of $M_n <$ 13 000 g mol^{-1} in the case of the *n*-octadecyl hydrophobic end group (Figure 8). Note that the polymer C_{18}-PiPrOx-OH-13K, which does not micellizes, readily crystallizes from hot water as well.

Temperature-Dependent Properties of Aqueous C_{18}-PiPrOx-C_{18} Solutions. A study by turbidimetry of aqueous solutions of three C_{18}-PiPrOx-C_{18} samples was performed for solutions in the dilute regime (1.0 g L^{-1}), which are conditions for which the polymers predominantly exist in the form of flower

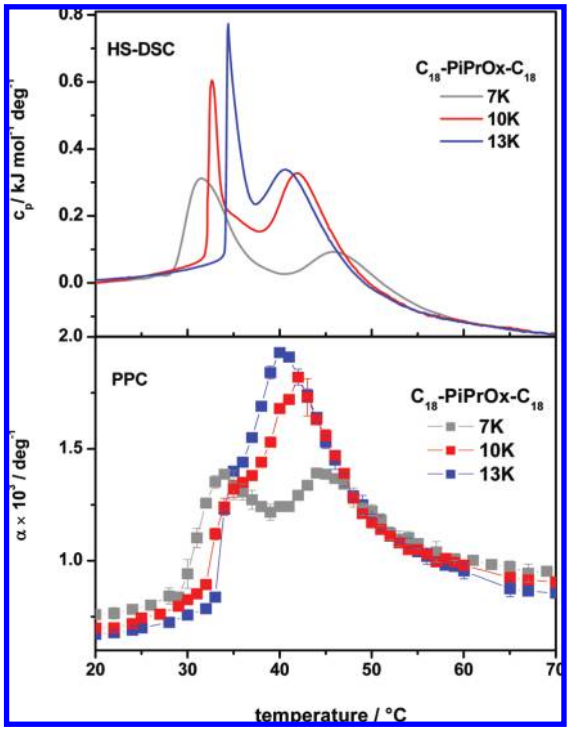

Figure 11. (top) Microcalorimetric endotherms (polymer concentration: 1.0 g L^{-1}) and (bottom) temperature dependence of the coefficient of thermal expansion (α) (polymer concentration: 2.5 g L^{-1}) of aqueous solutions of C_{18}-PiPrOx-C_{18}.

micelles with hydrodynamic radii on the order of ~10 nm[19] (Table 1). The solution cloud points of the three telechelic PiPrOx samples are lower than those of their unmodified counterparts (Table 2). The T_{cp} depression upon end-group modification is the largest (~16 °C) in the case of the shortest polymer (C_{18}-PiPrOx-C_{18} 7K). The T_{cp} of aqueous C_{18}-PiPrOx-C_{18} solutions decreases with increasing polymer concentration, as in the case of solutions of unmodified and semitelechelic PiPrOx. For example, the T_{cp} of a C_{18}-PiPrOx-C_{18} 10K solution drops by nearly 15 °C as the polymer concentration increases from 0.1 to ~1.0 g L^{-1}. It remains constant upon further increase in polymer concentration up to 10 g L^{-1}.

HS-DSC and PPC scans recorded for aqueous solutions of the three C_{18}-PiPrOx-C_{18} samples are presented in Figure 11. Each scan features two maxima, T_{Lo} and T_{Hi} (Table 2). On the basis of the analysis described in detail in the case of the semitelechelic polymers, we assigned the transition at T_{Hi} to the dehydration/collapse of the PiPrOx chains and the transition at T_{Lo} to a change in the packing/ordering of the *n*-octadecyl chains in the core of the micelles. There is a striking difference in the sharpness of the T_{Lo} transition for solutions of C_{18}-PiPrOx-C_{18} 13K and C_{18}-PiPrOx-C_{18} 10K, compared to the T_{Lo} transition of C_{18}-PiPrOx-C_{18} 7K and of the semitelechelic HM-PiPrOx solutions (Figures 6 and 11). The enhanced sharpness indicates an enhancement in the cooperativity of the transition. We know from previous DLS and SAXS measurements[19] that aqueous solutions of C_{18}-PiPrOx-C_{18} 7K contain solely flower micelles (R_H ~ 8 nm) with no measurable contribution of larger intermicellar associates. However, in solutions of C_{18}-PiPrOx-C_{18} 10K and 13K, large objects (R_H ~ 100 nm) presumed to be clusters of micelles coexist with the flower micelles and this, well below the solutions cloud points. In solutions of flower micelles, concentration fluctuations promote intermicellar connections via bridging of micelles through chains having

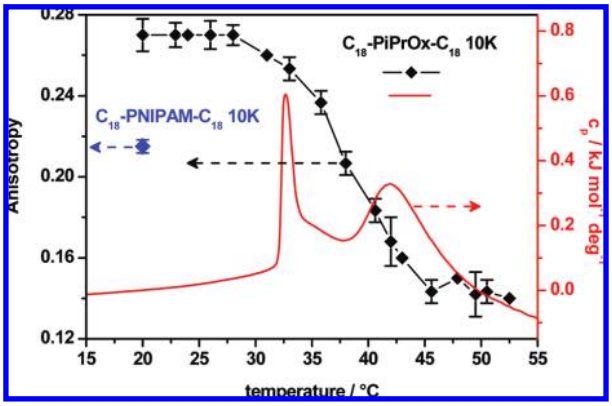

Figure 12. Changes in fluorescence anisotropy of DPH (black diamond) as a function of temperature (from ref 19) and microcalorimetric endotherm (from this study) for an aqueous solution of C_{18}-PiPrOx-C_{18} 10K (polymer concentration: 1.0 g L^{-1}). The fluorescence anisotropy of DPH in cold aqueous solution of C_{18}-PNIPAM-C_{18} 10K (1.0 g L^{-1}, 20 °C) is represented by the blue diamond symbol.

their end groups in the cores of two different micelles. This bridging mechanism has been demonstrated in studies of telechelic HM-PEO[59] and telechelic HM-PNIPAM solutions.[60,61] The enhanced cooperativity of the T_{Lo} endotherm for solutions of C_{18}-PiPrOx-C_{18} 10K and 13K, compared to C_{18}-PiPrOx-C_{18} 7K, may reflect the fact that the restructuring of the *n*-octadecyl chains in the micellar core is accompanied by intermicellar bridging. In the case of C_{18}-PiPrOx-C_{18} 10K and 13K, the connections can occur between micelles interlocked in close proximity within clusters, while in the case of C_{18}-PiPrOx-C_{18} 7K, the processus involves bridging between isolated flower micelles upon diffusive contact between micelles. We note also that the ΔH_{Lo} values, computed in terms of C_{18} units, decrease with decreasing polymer molecular weight range, unlike the situation observed for semitelechelic HM-PiPrOx samples (Table 2). This trend may be attributed to the presence of dangling C_{18} segments, which are not incorporated in the micellar core.

A close examination of fluorescence depolarization measurements,[19] using diphenylhexatriene (DPH) as a probe of the microfluidity of a given environment, provides further evidence for the occurrence of a phase change in the core of the micelles. DPH is a rigid nonpolar molecule which is solubilized preferentially in hydrophobic environments. It is used extensively to assess the microviscosity within lipid bilayers[62] and in the core of surfactant or polymer micelles.[63] The DPH anisotropy, r_0, ranges from ~0 in low-viscosity liquids such as tetrahydrofuran to ~0.37, its limiting value in rigid media. An overlay of the temperature dependence of the DPH anisotropy in aqueous C_{18}-PiPrOx-C_{18} 10K (data taken from ref 19, Figure 12) and the microcalorimetry trace recorded for the same polymer solution reveals that the decrease in anisotropy, or increase in fluidity experienced by the probe, coincides with the T_{Lo} transition, providing further support to the mechanism we associate with this transition. We note that r_0 remains constant upon heating until the temperature exceeds the onset temperature of the low-temperature transition (27 °C). From this temperature and until 45 °C, the anisotropy decreases, indicating that the DPH environment becomes increasingly more fluid. It reaches a plateau value of ~0.14 as the solution temperature exceeds 45 °C, i.e., past the high-temperature transition (T_{Hi} = 42.1 °C). Fluorescence depolarization studies carried out

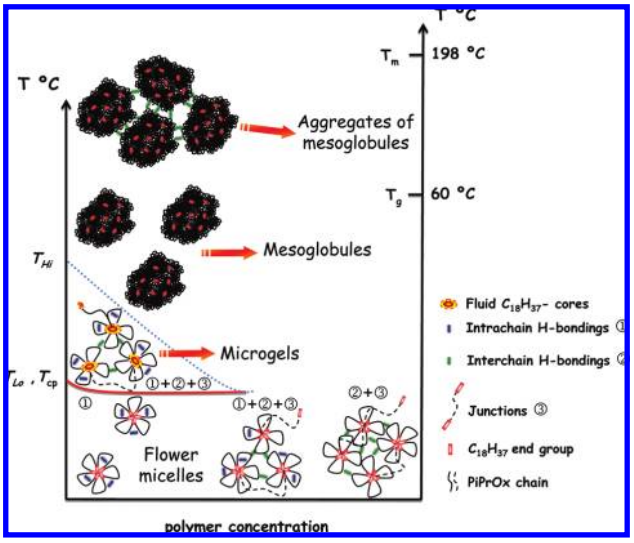

Figure 13. Temperature−concentration phase diagram of C_{18}-PiPrOx-C_{18} 10K/water system. It pictorially shows cloud point (red) and collapse transition (blue) lines which correspond to the aggregation and dehydration of the polymer, respectively, together with associated structures such as flowers connected by bridge chains, microgels, and aggregates of mesoglobules.

with solutions of semitelechelic HM-PiPrOx samples revealed similar trends.[19]

In a final set of experiments, we incubated solutions of telechelic HM-PiPrOx at 70 °C for 24 h. Unexpectedly, the solution, which was turbid at high temperature, recovered its limpidity upon cooling below T_{Lo}. We knew from DSC scans that telechelic HM-PiPrOxs in the bulk are semicrystalline polymers with a melting point of 198 °C (Figure SI.3). To establish firmly that the samples did not crystallize from hot water, we recorded XRD traces of the powder recovered after lyophilization of the cooled solutions. They were featureless (Figure 10). The absence of crystalline fibers was confirmed also by TEM imaging of the cooled sample (Figure SI.5). The reluctance to crystallize of the telechelic sample must originate in its assembly, in cold water, in the form of flower micelles. We reported previously, on the basis of fluorescence depolarization measurements,[19] that the hydrophobic core of telechelic HM-PiPrOx flower micelles is preserved upon heat-triggered collapse and aggregation of the PiPrOx chains. The corollary of this observation is that the dehydrated chains must adopt a "crumbled loop" conformation within the separated polymer-rich phase. The motion of the chains is restricted in this environment. Reorganization toward chain alignment and crystallization cannot occur, at least under the experimental conditions used here.

In Figure 13, we represent the phase diagram of the telechelic HM-PiPrOx in water, constructed based on information gathered in this study and on scattering data reported previously.[19] In the low-temperature dilute regime, isolated hydrated flower micelles form, together with small clusters of interlinked micelles. In solutions heated within the T_{Lo} to T_{Hi} range, hydrated microgels form by interlinking of individual flower micelles connected by bridging chains. The PiPrOx loops of the micelles dehydrate and collapse in solutions of $T > T_{Hi}$, forcing the microgels to shrink and aggregate into large objects in which the hydrophobic core, in its fluid state is mostly preserved. Within these objects, the crystallization of the PiPrOx chain does not occur. The overall process is reversible: intact flower micelles are recovered by cooling the solution to room temperature.

Conclusions

This study demonstrates that the decoupling between the T_{cp} and T_M in the phase diagram of telechelic HM-polymers/water systems is not limited to the HM-PEO/water and HM-PNIPAM/water systems and that it occurs also in aqueous solutions of HM-PiPrOx. Moreover, the same decoupling is observed in aqueous solutions of the semitelechelic HM-PiPrOx samples, for which intermicellar clustering via bridging chains is impossible. The turbidity of semitelechelic HM-PiPrOx solutions in the T_{cp} to T_M (or T_{Hi} according to the notation adopted here) temperature window was attributed to the formation of large objects, either cylindrical objects or clusters of micelles which may be linked via bridging water molecules. Temperature-dependent SAXS measurements in progress are expected to clarify this point. One unexpected result of the study is that in solutions of both semitelechelic and telechelic HM-PiPrOx the onset of turbidity is accompanied by a phase transition of the hydrophobic core, detected by an endotherm in the HS-DSC scans, unlike the situation in solutions of telechelic HM-PNIPAM samples for which the enhancement in turbidimetry was not detected by microcalorimetry (see Figure 1). The fact that the T_{Lo} transition was not detected in calorimetry studies of solutions of telechelic HM-PNIPAM implies either that the two transitions occur at the same temperature in the case of telechelic HM-PNIPAM or that the micellar core of PNIPAM flower micelles does not undergo a rigid-fluid phase transition, presumably due to the fact that it forms a fluid phase already at 20 °C. The latter interpretation is strengthened by data taken from fluorescence depolarization measurements with DPH. The r_0 value recorded for DPH solubilized in the core of C_{18}-PiPrOx-C_{18} 10K flower micelles in water at 20 °C is ~0.275, whereas for DPH solubilized in aqueous C_{18}-PNIPAM-C_{18} 10K at 20 °C it is significantly lower (~0.22), confirming that in cold (20 °C) water the core of C_{18}-PNIPAM-C_{18} 10K micelles is more fluid than that of aqueous C_{18}-PiPrOx-C_{18} 10K.[64] The peculiar properties of the PiPrOx, compared to its structural isomer PNIPAM is attributable to the presence, along the polymer backbone, of tertiary amide nitrogens, which, as in the case of peptides and peptoids, impose steric constraints, direct the interactions of the polymer with surrounding water molecules, and eventually triggers the crystallization of the polymer from hot water.

Our study also provides evidence that hydrophobic end-group modification of PiPrOx affects the propensity of the polymer to crystallize from hot water. Semitelechelic HM-PiPrOx samples crystallize from hot water in the form of fibrils polydisperse in length but uniform in width, reminiscent in structure to the rodlike micelles formed by certain amphiphilic diblock copolymers.[65] Remarkably, telechelic HM-PiPrOx samples resist crystallization from hot water. This resistance to crystallization must be taken as an indication that the loops formed by polymer chains captured in the flower micelles that exist in cold water retain their topology in the aggregates formed upon heating telechelic HM-PiPrOx samples above their phase transition temperature. This behavior is rather unique, since other end-modifications of the PiPrOx chains reported so far, for example grafting onto polysaccharides,[66] do not hinder its crystallization from hot water.

Acknowledgment. The authors thank Dr. P. Kujawa for critical reading of the manuscript and for valuable comments and Dr. T. Koga (Kyoto University, Japan) for sharing data and helpful discussions. Also, we thank Dr. E. Hutter and Mr. A. Moquin for technical support during TEM preparation sample and imaging and Mr. Q. Zhang for help during XRD measurements. This work was supported by a research grant of the Natural Sciences and Engineering Research Council of Canada

to F.M.W. and by the FQRNT Center for Self-Assembled Chemical Structures.

Supporting Information Available: HS-DSC thermograms showing the effect of the heating rate on the position of T_M (T_{Lo} and T_{Hi}); DSC traces of Me-PiPrOx-OH 10K and C_{18}-PiPrOx-C_{18} 10K in bulk; light optical microscopy images presenting the formation of spherulites upon cooling melted samples of Me-PiPrOx-OH 10K and C_{18}-PiPrOx-C_{18} 10K; TEM images of the product obtained after a 24 h incubation at 70 °C of an aqueous solution of C_{18}-PiPrOx-C_{18} 10K (10 g L^{-1}); experimental protocol employed in the fluorescence anisotropy measurements. This material is available free of charge via the Internet at http://pubs.acs.org.

References and Notes

(1) Ball, P. *Chem. Rev.* **2008**, *108* (1), 74–108.
(2) Berret, J. F.; Calvet, D.; Collet, A.; Viguier, M. *Curr. Opin. Colloid Interface Sci.* **2003**, *8* (3), 296–306.
(3) Winnik, M. A.; Yekta, A. *Curr. Opin. Colloid Interface Sci.* **1997**, *2* (4), 424–436.
(4) Sprakel, J.; Besseling, N. A. M.; Leermakers, F. A. M.; Cohen Stuart, M. A. *J. Phys. Chem. B* **2007**, *111* (11), 2903–2909.
(5) Cass, M. J.; Heyes, D. M.; Blanchard, R. L.; English, R. J. *J. Phys.: Condens. Matter* **2008**, *20*, 33.
(6) Sprakel, J.; Besseling, N. A. M.; Cohen, M. A.; Leermakers, F. A. M. *Eur. Phys. J. E* **2008**, *25* (2), 163–173.
(7) Yekta, A.; Xu, B.; Duhamel, J.; Adiwidjaja, H.; Winnik, M. A. *Macromolecules* **1995**, *28* (4), 956–966.
(8) Alami, E.; Almgren, M.; Brown, W.; François, J. *Macromolecules* **1996**, *29* (6), 2229–2243.
(9) Tanaka, F.; Edwards, S. F. *Macromolecules* **1992**, *25* (5), 1516–1523.
(10) François, J.; Beaudoin, E.; Borisov, O. *Langmuir* **2003**, *19* (24), 10011–10018.
(11) Koga, T.; Tanaka, F. *Eur. Phys. J. E* **2005**, *17* (2), 115–118.
(12) *Associative Polymers in Aqueous Solution*; Glass, J. E., Ed.; American Chemical Society: Washington, DC, 2000; Vol. *765*.
(13) Kaczmarski, J. P.; Glass, J. E. *Macromolecules* **1993**, *26* (19), 5149–5156.
(14) Kadam, V. S.; Badiger, M. V.; Wadgaonkar, P. P.; Ducouret, G.; Hourdet, D. *Polymer* **2008**, *49* (21), 4635–4646.
(15) Calvet, D.; Collet, A.; Viguier, M.; Berret, J.-F.; Serero, Y. *Macromolecules* **2003**, *36* (2), 449–457.
(16) Rufier, C.; Collet, A.; Viguier, M.; Oberdisse, J.; Mora, S. *Macromolecules* **2008**, *41* (15), 5854–5862.
(17) Alami, E.; Abrahmsén-Alami, S.; Vasilescu, M.; Almgren, M. *J. Colloid Interface Sci.* **1997**, *193* (2), 152–162.
(18) Weberskirch, R.; Preuschen, J.; Spiess, H. W.; Nuyken, O. *Macromol. Chem. Phys.* **2000**, *201* (10), 995–1007.
(19) Obeid, R.; Maltseva, E.; Thünemann, A. F.; Tanaka, F.; Winnik, F. M. *Macromolecules* **2009**, *42* (6), 2204–2214.
(20) Huber, S.; Hutter, N.; Jordan, R. *Colloid Polym. Sci.* **2008**, *286* (14−15), 1653–1661.
(21) Kubowicz, S.; Thünemann, A. F.; Weberskirch, R.; Mohwald, H. *Langmuir* **2005**, *21* (16), 7214–7219.
(22) Kujawa, P.; Segui, F.; Shaban, S.; Diab, C.; Okada, Y.; Tanaka, F.; Winnik, F. M. *Macromolecules* **2006**, *39* (1), 341–348.
(23) Heskins, M.; Guillet, J. E. *Macromol. Sci. Chem. A2* **1968**, 1441–1455.
(24) Litt, M.; Rahl, F.; Roldan, L. G. *J. Polym. Sci., Part A2* **1969**, *7*, 463–473.
(25) Kobayashi, S.; Saegusa, T. In *Ring-Opening Polymerization*; Ivin, K. J., Saegusa, T., Eds.; Elsevier Applied Science: Essex, UK, 1984; Vol. *2*, pp 761−780.
(26) Park, J. S.; Akiyama, Y.; Winnik, F. M.; Kataoka, K. *Macromolecules* **2004**, *37* (18), 6786–6792.
(27) Diab, C.; Akiyama, Y.; Kataoka, K.; Winnik, F. M. *Macromolecules* **2004**, *37* (7), 2556–2562.
(28) Gaertner, F. C.; Luxenhofer, R.; Blechert, B.; Jordan, R.; Essler, M. *J. Controlled Release* **2007**, *119* (3), 291–300.
(29) Jordan, R.; Martin, K.; Rader, H. J.; Unger, K. K. *Macromolecules* **2001**, *34* (26), 8858–8865.
(30) Volet, G.; Chanthavong, V.; Wintgens, V.; Amiel, C. *Macromolecules* **2005**, *38* (12), 5190–5197.
(31) Ivanova, R.; Komenda, T.; Bonne, T. B.; Ludtke, K.; Mortensen, K.; Pranzas, P. K.; Jordan, R.; Papadakis, C. M. *Macromol. Chem. Phys.* **2008**, *209* (21), 2248–2258.
(32) Binder, W. H.; Gruber, H. *Macromol. Chem. Phys.* **2000**, *201* (9), 949–957.
(33) Park, J. S.; Kataoka, K. *Macromolecules* **2006**, *39* (19), 6622–6630.
(34) Meyer, M.; Antonietti, M.; Schlaad, H. *Soft Matter* **2007**, *3* (4), 430–431.
(35) Demirel, A. L.; Meyer, M.; Schlaad, H. *Angew. Chem., Int. Ed.* **2007**, *46* (45), 8622–8624.
(36) Chen, F. P.; Ames, A. E.; Taylor, L. D. *Macromolecules* **1990**, *23* (21), 4688–4695.
(37) Okhapkin, I. A.; Makhaeva, E. E.; Khokhlov, A. R. *Adv. Polym. Sci.* **2006**, *195*, 177−210.
(38) Tanaka, A.; Kobayashi, D.; Senoo, K.; Obata, H. *Biosci., Biotechnol., Biochem.* **1999**, *63* (2), 438–442.
(39) Kujawa, P.; Winnik, F. M. *Macromolecules* **2001**, *34* (12), 4130–4135.
(40) Lin, L. N.; Brandts, J. F.; Brandts, J. M.; Plotnikov, V. *Anal. Biochem.* **2002**, *302* (1), 144–160.
(41) Laukkanen, A.; Valtola, L.; Winnik, F. M.; Tenhu, H. *Macromolecules* **2004**, *37* (6), 2268–2274.
(42) Beezer, A. E.; Loh, W.; Mitchell, J. C.; Royall, P. G.; Smith, D. O.; Tute, M. S.; Armstrong, J. K.; Chowdhry, B. Z.; Leharne, S. A. *Langmuir* **1994**, *10* (11), 4001–4005.
(43) Nemethy, G.; Scheraga, H. A. *J. Chem. Phys.* **1964**, *41* (3), 680–689.
(44) Kresheck, G. C. *J. Phys. Chem. B* **1998**, *102* (34), 6596–6600.
(45) Sasisanker, P.; Oleinikova, A.; Weingartner, H.; Ravindra, R.; Winter, R. *Phys. Chem. Chem. Phys.* **2004**, *6* (8), 1899–1905.
(46) Blandamer, M. J.; Briggs, B.; Burgess, J.; Cullis, P. M.; Eaton, G. *J. Chem. Soc., Faraday Trans.* **1991**, *87* (8), 1169–1175.
(47) Mori, T.; Hirano, T.; Maruyama, A.; Katayama, Y.; Niidome, T.; Bando, Y.; Ute, K.; Takaku, S.; Maeda, Y. *Langmuir* **2009**, *25* (1), 48–50.
(48) Tiktopulo, E. I.; Uversky, V. N.; Lushchik, V. B.; Klenin, S. I.; Bychkova, V. E.; Ptitsyn, O. B. *Macromolecules* **1995**, *28* (22), 7519–7524.
(49) Ebel, H.; Grabitz, P.; Heimburg, T. *J. Phys. Chem. B* **2001**, *105* (30), 7353–7360.
(50) Heerklotz, H.; Tsamaloukas, A.; Kita-Tokarczyk, K.; Strunz, P.; Gutberlet, T. *J. Am. Chem. Soc.* **2004**, *126* (50), 16544–16552.
(51) Heerklotz, H.; Seelig, J. *Biophys. J.* **2002**, *82* (3), 1445–1452.
(52) Litt, M.; Rahl, F.; Roldan, L. G. *J. Polym. Sci., Polym. Phys.* **1969**, *7*, 463–473.
(53) Kujawa, P.; Tanaka, F.; Winnik, F. M. *Macromolecules* **2006**, *39* (8), 3048–3055.
(54) Messerly, J. F.; Guthrie, G. B.; Todd, S. S.; Finke, H. L. *J. Chem. Eng. Data* **1967**, *12* (3), 338–346.
(55) Naumann, C. A.; Brooks, C. F.; Fuller, G. G.; Lehmann, T.; Ruehe, J.; Knoll, W.; Kuhn, P.; Nuyken, O.; Frank, C. W. *Langmuir* **2001**, *17* (9), 2801–2806.
(56) Thünemann, A. F. Private communication.
(57) Shan, J.; Chen, J.; Nuopponen, M.; Tenhu, H. *Langmuir* **2004**, *20* (11), 4671–4676.
(58) Luo, S.; Xu, J.; Zhu, Z.; Wu, C.; Liu, S. *J. Phys. Chem. B* **2006**, *110* (18), 9132–9139.
(59) Chassenieux, C.; Nicolai, T.; Durand, D. *Macromolecules* **1997**, *30* (17), 4952–4958.
(60) Nojima, R.; Sato, T.; Qiu, X.; Winnik, F. M. *Macromolecules* **2008**, *41* (2), 292–294.
(61) Kujawa, P.; Watanabe, H.; Tanaka, F.; Winnik, F. M. *Eur. Phys. J. E* **2005**, *17* (2), 129–137.
(62) Shinitzky, M.; Barenholz, Y. *Biochim. Biophys. Acta* **1978**, *515* (4), 367–94.
(63) Ringsdorf, H.; Venzmer, J.; Winnik, F. M. *Macromolecules* **1991**, *24* (7), 1678–1686.
(64) The r_0 value for DPH in aqueous C_{18}-PNIPAM-C_{18} 10K solution was measured under conditions given in section SI.6 using a polymer synthesized by Drs. X.-P. Qiu and K. Shivaji Sharma (University of Montreal); unpublished results.
(65) Massey, J. A.; Temple, K.; Cao, L.; Rharbi, Y.; Raez, J.; Winnik, M. A.; Manners, I. *J. Am. Chem. Soc.* **2000**, *122* (47), 11577–11584.
(66) Morimoto, N.; Obeid, R.; Yamane, S.; Winnik, F. M.; Akiyoshi, K. *Soft Matter* **2009**, *5* (8), 1597–1600.